Electronic Supplementary Material (ESI) for Inorganic Chemistry Frontiers.

Supporting Information

Tetranuclear lanthanide complexes display significant slow magnetic relaxation with open hysteresis loop and magnetocaloric effect

Tian-Tian Wang, [a] Zi-Wei Che, [a] Ji-Tun Chen, [a] Han Yan, [a] Teng-Da Zhou, [a] Yi-Quan Zhang [b] and Wen-Bin Sun [*a]

[a] Key Laboratory of Functional Inorganic Material Chemistry Ministry of Education, School of Chemistry and Material Science Heilongjiang University, 74 Xuefu Road, Harbin 150080, P. R. China. *E-mail: wenbinsun@126.com*

[b] Jiangsu Key Laboratory for NSLSCS, School of Physical Science and Technology, Nanjing Normal University, Nanjing 210023, P. R. China. *E-mail: zhangyiquan@njnu.edu.cn*

Table S1 Crystallographic data for complexes **1**-**3**.

	1	**2**	**3**
Empirical formula	$C_{100}H_{100}Dy_4N_{12}O_{22}$	$C_{106}H_{114}Gd_4N_{14}O_{24}$	$C_{322}H_{372}Y_{12}N_{32}O_{78}$
Formula weight	2471.91	2597.10	7005.32
Crystal system	trigonal	trigonal	trigonal
Space group	R	R	R
Temperature (K)	212.95(10)	173	173(10)
a (Å)	41.5368(11)	41.4910(8)	41.2845(9)
b (Å)	41.5368(11)	41.4910(8)	41.2845(9)
c (Å)	16.4686(6)	16.4542(3)	16.3767(5)
α (°)	90	90	90
β (°)	90	90	90
γ (°)	120	120	120
V (Å^3)	24606.7(16)	24531.0(10)	24173.1(14)
ρ_{calc} (Mg m^{-3})	1.501	1.582	1.441
μ (mm^{-1})	2.771	16.118	3.451
F(000)	11016.0	11664.0	10824.0
Collected reflections	28613	36627	59106
Independent reflections	9590	9676	9596
*R*int	0.1115	0.0663	0.0723
R_1 [$I > 2\sigma(I)$]	0.0647	0.0512	0.0596
wR_2 (all data)	0.1801	0.1455	0.1921
Goodness of fit on F^2	1.030	1.016	1.030
CCDC number	2208476	2208475	2226681

Table S2 Selected bond lengths (Å) and angles (°) for complexes **1** and **3**.

Dy2-Dy1	3.8102(5)	Dy1-Dy1'	3.8094(7)
Dy2-O4	2.296(5)	Dy1-O1	2.305(5)
Dy2-O6	2.337(5)	Dy1-O1'	2.314(5)
Dy2-O3	2.243(5)	Dy1-O4	2.412(5)
Dy2-O7	2.308(5)	Dy1-O6	2.386(5)
Dy2-N1	2.533(7)	Dy1-O8	2.489(5)
Dy2-N4	2.565(6)	Dy1-O10	2.401(5)
Dy2-N6	2.505(6)	Dy1-O11	2.432(6)
Dy2-N3	2.498(6)	Dy1-O2	2.260(5)
O4-Dy2-Dy1	37.02(11)	O1-Dy1-O8	74.27(18)
O4-Dy2-O6	73.67(17)	O1'-Dy1-O8	78.46(18)
O4-Dy2-O7	83.73(17)	O1-Dy1-O10	89.47(18)
O4-Dy2-N6	74.11(19)	O1'-Dy1-O11	130.89(18)
O4-Dy2-N3	145.41(19)	O4-Dy1-Dy2	34.97(11)
O6-Dy2-Dy1	36.66(12)	O4-Dy1-Dy1'	99.35(11)

O6-Dy2-N1	119.82(19)	O4-Dy1-O8	115.33(18)
O6-Dy2-N4	145.7(2)	O4-Dy1-O11	75.50(18)
O6-Dy2-N6	145.2(2)	O6-Dy1-Dy2	35.78(11)
O6-Dy2-N3	74.70(19)	O6-Dy1-Dy1'	155.25(11)
O3-Dy2-Dy1	82.27(15)	O6-Dy1-O4	70.75(16)
O3-Dy2-O4	83.17(19)	O6-Dy1-O8	131.31(17)
O3-Dy2-O6	83.9(18)	O6-Dy1-O10	75.53(18)
O3-Dy2-O7	160.2(2)	O6-Dy1-O11	86.87(18)
O3-Dy2-N1	71.0(2)	O8-Dy1-Dy2	132.07(14)
O3-Dy2-N4	129.0(2)	O8-Dy1-Dy1'	73.41(13)
O3-Dy2-N6	79.5(2)	O10-Dy1-Dy2	73.31(13)
O3-Dy2-N3	107.0(2)	O10-Dy1-Dy1'	80.26(14)
O7-Dy2-Dy1	78.36(13)	O10-Dy1-O4	77.90(17)
O7-Dy2-N4	70.3(2)	O11-Dy1-Dy2	79.49(14)
O7-Dy2-N6	110.9(2)	O11-Dy1-Dy1'	113.19(14)
O7-Dy2-N3	76.5(2)	O11-Dy1-O8	52.9(2)
N1-Dy2-Dy1	147.57(14)	O2-Dy1-Dy2	105.99(13)
N1-Dy2-N4	71.4(2)	O2-Dy1-Dy1'	118.51(13)
N4-Dy2-Dy1	141.04(14)	O2-Dy1-O1'	85.33(18)
N3-Dy2-Dy1	110.19(14)	O2-Dy1-O8	87.04(19)
N3-Dy2-N6	139.6(2)	Dy1-O1-Dy1'	111.2(2)
Dy1'-Dy1-Dy2	130.507(15)	O1-Dy1-O1'	68.90(19)
O1-Dy1-Dy2	103.51(13)	O1'-Dy1-O4	128.90(16)
O1'-Dy1-Dy2	146.85(12)	O1-Dy1-O4	68.79(17)
O1'-Dy1-Dy1'	34.38(11)	O1'-Dy1-O6	138.06(16)
O1-Dy1-Dy1'	34.52(12)	O1-Dy1-O6	138.94(17)

Y1-Y1'	3.7886(9)	Y1-O1'	2.306(3)
Y1-Y2	3.7970(6)	Y2-O3	2.235(3)
Y1-O2	2.266(3)	Y2-O4	2.296(3)
Y1-O4	2.406(3)	Y2-O6	2.328(3)
Y1-O6	2.382(3)	Y2-O7	2.305(3)
Y1-O8	2.478(4)	Y2-N1	2.512(4)
Y1-O10	2.370(3)	Y2-N3	2.497(4)
Y1-O11	2.409(3)	Y2-N4	2.553(4)
Y1-O1	2.299(3)	Y2-N6	2.487(4)
Y1'-Y1-Y2	130.578(19)	O3-Y2-Y1	82.10(9)
O2-Y1-Y1'	118.51(9)	O3-Y2-O4	83.09(12)
O2-Y1-Y2	105.94(9)	O3-Y2-O6	83.59(12)
O2-Y1-O10	97.39(12)	O3-Y2-O7	159.26(13)
O2-Y1-O11	97.12(13)	O3-Y2-N1	71.30(14)

O2-Y1-O1	150.63(12)	O3-Y2-N3	106.97(13)
O2-Y1-O1'	85.14(12)	O3-Y2-N4	129.69(14)
O2-Y1-C6	96.42(15)	O3-Y2-N6	79.53(14)
O4-Y1-Y1'	99.16(8)	O4-Y2-Y1	37.15(8)
O4-Y1-Y2	35.18(7)	O4-Y2-O6	73.90(11)
O6-Y1-O8	131.16(12)	O4-Y2-O7	83.21(12)
O6-Y1-O1'	86.71(12)	O4-Y2-N1	148.37(13)
O6-Y1-C6	111.30(15)	O4-Y2-N3	145.85(13)
O8-Y1-Y1'	73.25(9)	O4-Y2-N4	114.80(12)
O8-Y1-Y2	132.18(10)	O4-Y2-N6	74.28(13)
O8-Y1-C6	27.20(15)	O6-Y2-Y1	36.76(8)
O10-Y1-Y1'	80.59(9)	O6-Y2-N1	119.68(13)
O10-Y1-Y2	73.05(9)	O6-Y2-N3	74.95(12)
O10-Y1-O4	77.67(12)	O6-Y2-N4	145.24(13)
O10-Y1-O6	75.52(12)	O6-Y2-N6	145.43(13)
O11-Y1-O8	52.91(13)	O7-Y2-Y1	77.57(9)
O11-Y1-C6	26.29(15)	O7-Y2-O6	77.69(12)
O1'-Y1-Y1'	34.59(8)	O7-Y2-N1	126.15(13)
O1-Y1-Y1'	34.72(8)	O7-Y2-N3	76.80(13)
O1'-Y1-Y2	146.88(9)	O7-Y2-N4	70.53(14)
O1-Y1-Y2	103.40(8)	O7-Y2-N6	111.45(14)
O1-Y1-O4	68.47(11)	N1-Y2-Y1	147.67(10)
O1'-Y1-O4	128.86(11)	N1-Y2-N4	71.65(14)
O1-Y1-O6	138.94(11)	N3-Y2-Y1	110.51(10)
O1'-Y1-O6	138.06(11)	N3-Y2-N1	62.54(14)
O1'-Y1-O8	78.40(13)	N3-Y2-N4	84.28(13)
O1-Y1-O8	74.14(12)	N4-Y2-Y1	140.66(10)
O1-Y1-O10	89.79(12)	N6-Y2-Y1	110.52(10)
O1'-Y1-O10	74.64(12)	N6-Y2-N1	82.88(14)
O1'-Y1-O11	130.88(13)	N6-Y2-N3	138.96(14)
O1-Y1-O11	89.39(12)	O1-Y1-O1'	69.31(13)

Table S3 Selected bond lengths (Å) and angles (°) for complex **2**.

Gd2-O1	2.365(4)	Gd1-O1	2.414(4)
Gd2-O3	2.331(4)	Gd1-O2	2.350(4)
Gd2-O5	2.284(4)	Gd1-O2[1]	2.331(4)
Gd2-O9	2.345(4)	Gd1-O3	2.437(4)
Gd2-N1	2.552(5)	Gd1-O4	2.308(4)
Gd2-N2	2.519(5)	Gd1-O6	2.430(4)
Gd2-N3	2.519(5)	Gd1-O7	2.509(4)

Gd2-N4	2.583(5)	Gd1-O8	2.463(4)
O1-Gd2-N1	118.88(14)	N2-Gd2-N4	85.23(16)
O1-Gd2-N2	74.11(15)	N3-Gd2-N1	83.64(16)
O1-Gd2-N3	145.48(16)	N3-Gd2-N4	62.82(18)
O1-Gd2-N4	145.61(16)	O1-Gd1-Gd1'	155.23(9)
O3-Gd2-O1	74.65(13)	O1-Gd1-O3	71.90(13)
O3-Gd2-O9	83.53(14)	O1-Gd1-O6	75.09(14)
O3-Gd2-N1	148.13(15)	O1-Gd1-O7	131.94(14)
O3-Gd2-N2	145.91(15)	O1-Gd1-O8	87.16(14)
O3-Gd2-N3	73.52(15)	O2-Gd1-Gd1'	34.52(9)
O3-Gd2-N4	114.34(15)	O2'-Gd1-Gd1'	34.84(9)
O5-Gd2-O1	83.75(14)	O2'-Gd1-O1	137.86(13)
O5-Gd2-O3	83.22(14)	O2-Gd1-O1	138.74(13)
O5-Gd2-O9	160.01(15)	O2'-Gd1-O2	69.36(15)
O5-Gd2-N1	70.82(15)	O2'-Gd1-O3	128.41(13)
O5-Gd2-N2	106.51(15)	O2-Gd1-O3	67.46(13)
O5-Gd2-N3	79.58(16)	O2-Gd1-O6	89.17(15)
O5-Gd2-N4	129.11(16)	O2'-Gd1-O6	75.27(14)
O9-Gd2-O1	78.34(14)	O2'-Gd1-O7	78.55(15)
O9-Gd2-N1	126.04(16)	O2-Gd1-O7	73.23(15)
O9-Gd2-N2	77.14(16)	O2-Gd1-O8	89.48(15)
O9-Gd2-N3	110.74(17)	O2'-Gd1-O8	130.63(14)
O9-Gd2-N4	70.32(16)	O3-Gd1-Gd1'	98.18(9)
N1-Gd2-N4	72.02(16)	O3-Gd1-O7	113.49(15)
N2-Gd2-N1	62.49(16)	O3-Gd1-O8	75.58(13)
N2-Gd2-N3	139.74(16)	O4-Gd1-Gd1'	119.49(10)

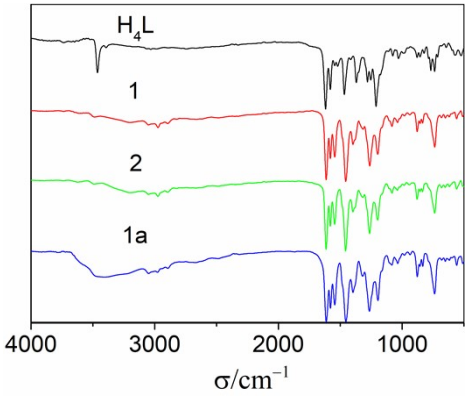

Fig. S1 Infrared spectra for H_4L, **1**, **2** and **1a**.

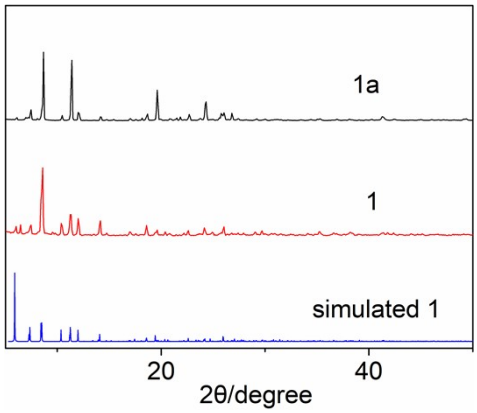

Fig. S2 Experimental and simulated X-ray powder diffraction patterns for **1** and **1a**.

As shown in Fig. S2, the data are slight inconsistencies between experimental and simulated X-ray powder diffraction patterns before 10 degrees, this is probably because there are still solvent molecules that have not been identified (the task of fully identifying solvent molecules in the lattice is not easy). In addition, due to the presence of solvent molecules in the complex, some of them may be lost during the PXRD testing process, which most likely lead to some difference between the experimental and simulated results.

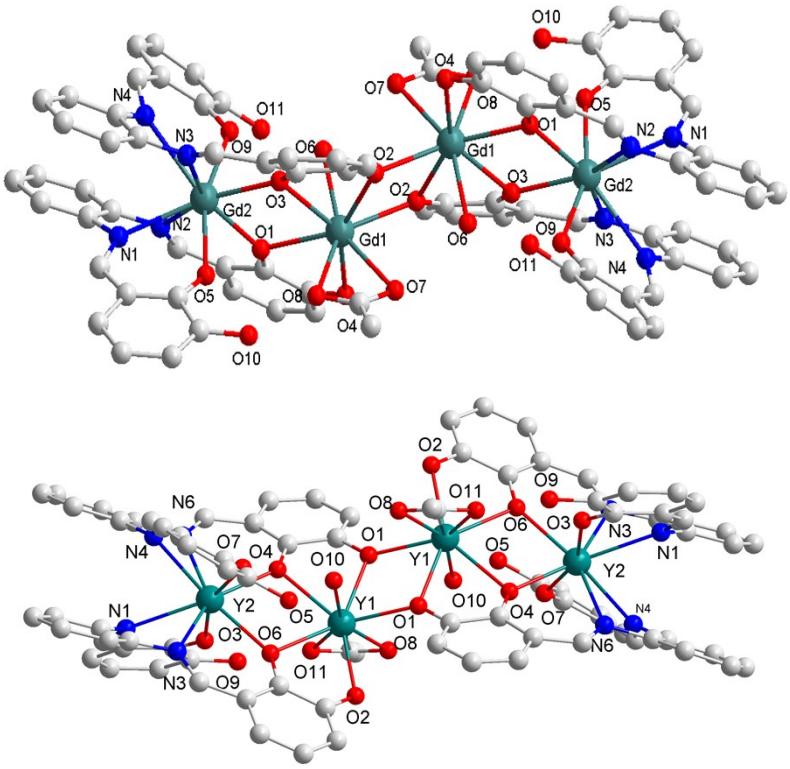

Fig. S3 Structure of complexes **2** and **3.**

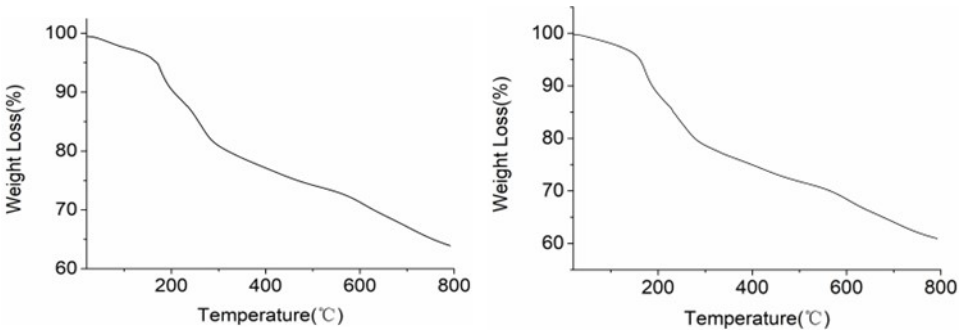

Fig. S4 TG curves of complexes **1** (left) and **2** (right).

Crystals of **1** and **2** have been selected for the thermogravimetric analysis in the experimental range of 20–800 degree. For **1**, the initial phase may be due to the loss of two acetonitrile molecules before 140 degree (found as 3.4 wt%, calculated as 3.3 wt%), which is consistent with the electron counts obtained by SQUEEZE. For **2**, the initial phase may be due to the loss of four acetonitrile molecules and two methanol molecules before 180 degree (found as 8.7 wt%, calculated as 8.8 wt%), which is consistent with the electron counts obtained by SQUEEZE.

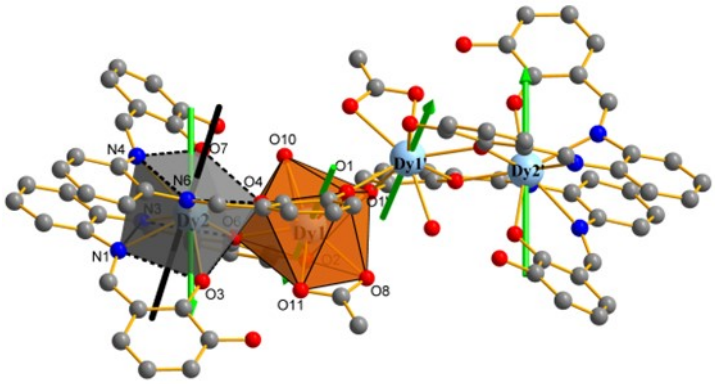

Fig. S5 Estimated coordination polyhedral surrounding Dy2 (Square antiprism) and Dy1 (Triangular dodecahedron). The solid black line is the axis of symmetry of the pseudo square antiprism. Calculated orientations of the local main magnetic axes on Dy^{III} ions of complex **1** in their ground KDs.

Table S4 Continuous Shape Measures (CShMs) of the coordination geometry for Dy^{III} ion in complex **1** (CShMs values calculated with the Shape program). The CShMs values indicated the proximity to the ideal polyhedron, thus, CShMs = 0 corresponds to the non-distorted polyhedron. The three closer ideal geometries to the real complexes are listed and below are the symmetry and description for each polyhedron.

	CShMs	Polyhedron
Dy1	1.491	TDD-8 D_{2d} Triangular dodecahedron
	3.485	BTPR-8 C_{2v} Biaugmented trigonal prism
	3.577	JSD-8 D_{2d} Snub diphenoid J84
Dy2	1.257	SAPR-8 D_{4d} Square antiprism
	2.299	TDD-8 D_{2d} Triangular dodecahedron
	2.518	BTPR-8 C_{2v} Biaugmented trigonal prism

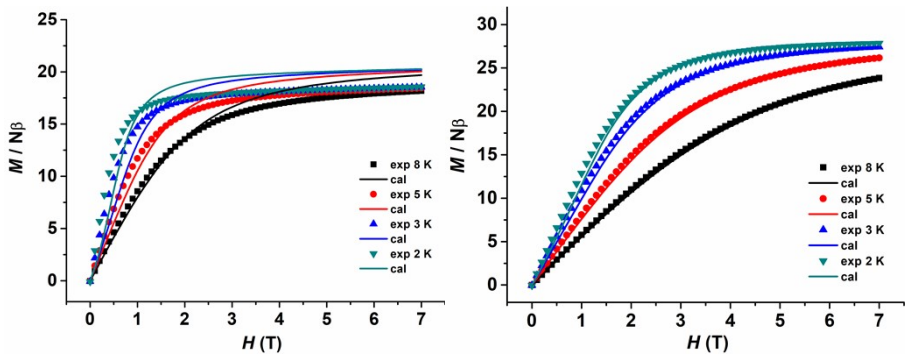

Fig. S6 Field dependences of magnetization in the field range 0-70 kOe for complexes **1** and **2** at 2, 3, 5 and 8 K.

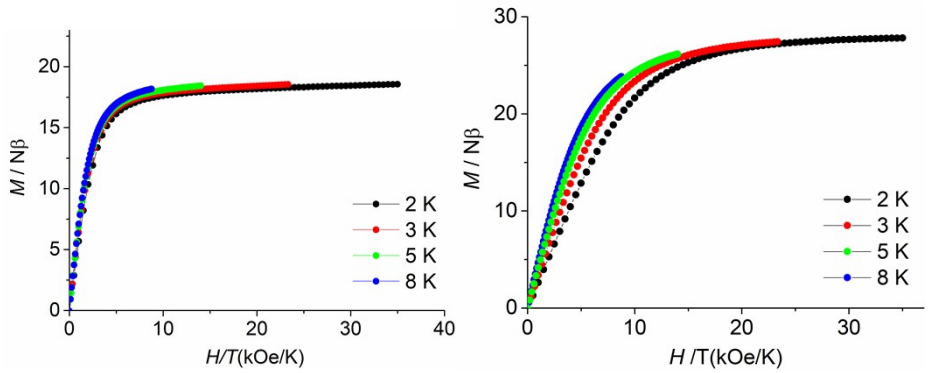

Fig. S7 Magnetization *M* vs *H*/*T* curves of complexes **1** and **2** at 2, 3, 5 and 8 K.

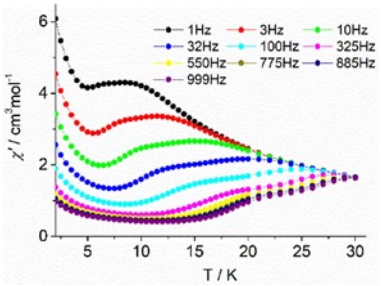

Fig. S8 Temperature dependence of the in-phase (χ') ac susceptibility in the temperature range 2-30 K of complex **1** under 0 Oe.

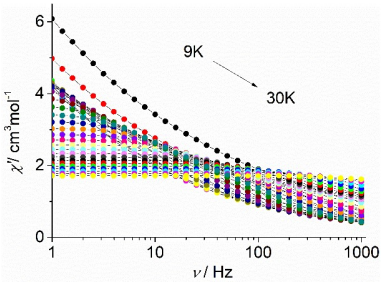

Fig. S9 Frequency dependence of the in-phase (χ') ac susceptibility in the temperature range 9-30 K of complex **1** under 0 Oe.

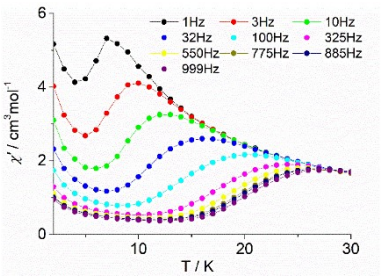

Fig. S10 Temperature dependence of the in-phase (χ') ac susceptibility in the temperature range 2-30 K of complex **1** under 1500 Oe.

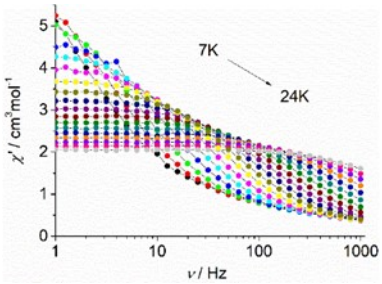

Fig. S11 Frequency dependence of the in-phase (χ') ac susceptibility in the temperature range 7-24 K of complex **1** under 1500 Oe.

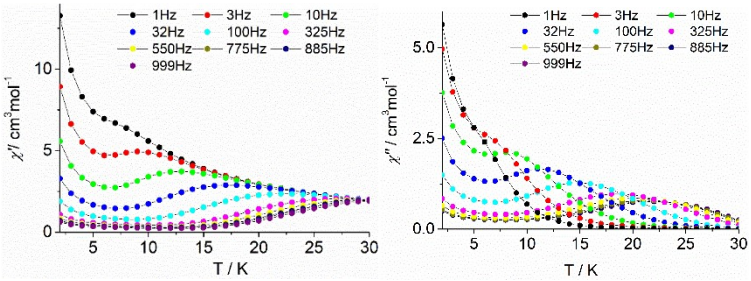

Fig. S12 Temperature dependence of the in-phase (χ') ac susceptibility (left) and the out-of-phase (χ'') ac susceptibility (right) in the temperature range 2-30 K of **1a** under 0 Oe.

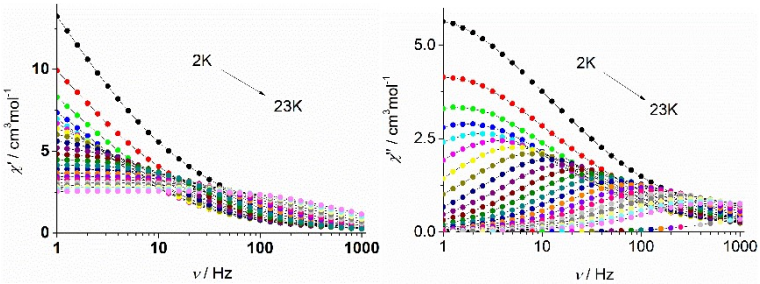

Fig. S13 Frequency dependence of the in-phase (χ') ac susceptibility (left) and the out-of-phase (χ'') ac susceptibility (right) in the temperature range 2-23 K of **1a** under 0 Oe.

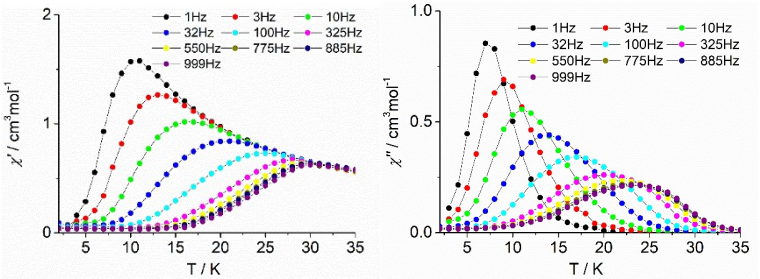

Fig. S14 Temperature dependence of the in-phase (χ') ac susceptibility (left) and the out-of-phase (χ'') ac

susceptibility (right) in the temperature range 2-35 K of **1a** under 1500 Oe.

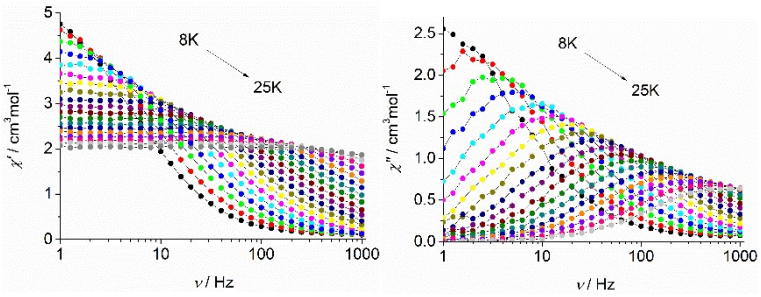

Fig. S15 Frequency dependence of the in-phase (χ′) ac susceptibility (left) and the out-of-phase (χ′′) ac susceptibility (right) in the temperature range 8-25 K of **1a** under 1500 Oe.

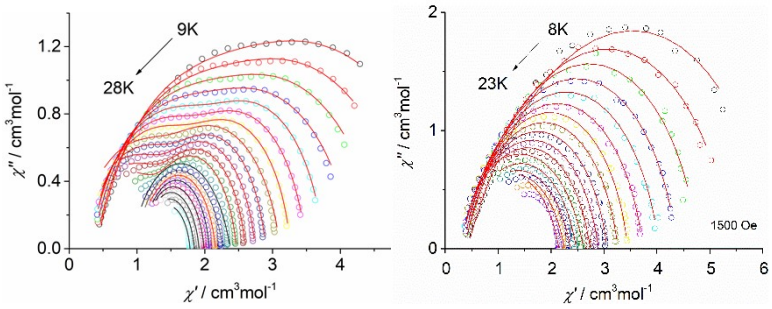

Fig. S16 Cole-Cole plots for **1** under 0 Oe (left) and 1500 Oe (right). The solid lines are the best fit for the generalized Debye model.

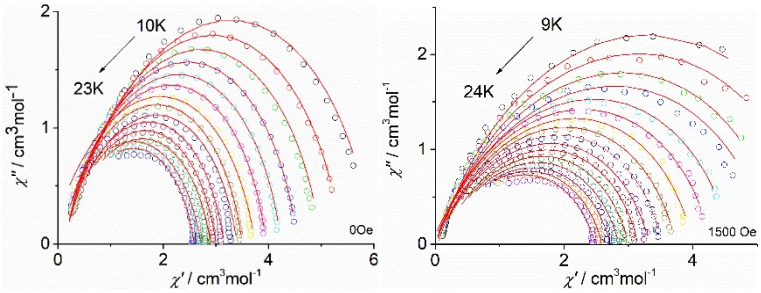

Fig. S17 Cole-Cole plots for **1a** under 0 Oe (left) and 1500 Oe (right). The solid lines are the best fit for the generalized Debye model.

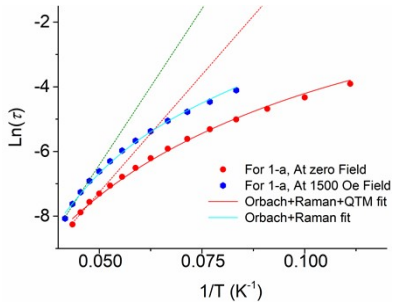

Fig. S18 Ln (τ) curves of *1/T* at 0 and 1500 Oe fields. The solid red line represents the fitting of frequency-dependent data by Eqn. (1) at 0 Oe dc field. The blue line represents the fitting of frequency-dependent data to **1a** using Eqn. (2) at 1500 Oe dc field. The dotted lines in green and red represent the pure Arrhenius fit of **1a** in the high-temperature linear region at 0 and 1500 Oe dc fields.

Table S5 Best fitted parameters (χ_S, χ_T, τ_1, τ_2, α_1, α_2 and β) with the extended Debye model featuring two relaxation times for complex **1** at 0 Oe in the temperature range 9-28 K.

T/ K	χ_S / cm^3 mol^{-1}	χ_T / cm^3 mol^{-1}	τ_1/s	α_1	τ_2/s	α_2	β
9	0.42934	5.30892	0.00622	0.23000	0.09187	0.35045	0.31000
10	0.38729	4.70532	0.00427	0.22996	0.06159	0.30578	0.36842
11	0.36425	4.08197	0.00344	0.23000	0.04840	0.17041	0.51613
12	0.17041	3.72316	0.00248	0.22988	0.03425	0.13226	0.55269
13	0.33279	3.41852	0.00159	0.19393	0.02257	0.13433	0.51662
14	0.28642	3.20000	0.00121	0.22447	0.01693	0.10993	0.56128
15	0.31016	2.95005	0.00080	0.18163	0.01157	0.11357	0.51759
16	0.27607	2.80001	0.00053	0.18626	0.00827	0.12534	0.50399
17	0.29486	2.58360	0.00046	0.22999	0.00687	0.06388	0.57830
18	0.33517	2.38887	0.00033	0.22998	0.00514	0.05801	0.56849
19	0.19602	2.40006	0.00014	0.23000	0.00269	0.10675	0.51773
20	0.33396	2.13007	0.00011	0.22981	0.00256	0.09168	0.50275
21	0.27766	2.09790	0.00000	0.23000	0.00113	0.21729	0.69735
22	0.25969	2.00574	0.00000	0.20266	0.00094	0.21100	0.64296
23	0.26541	1.89460	0.00000	0.22369	0.00079	0.15240	0.42212
24	0.04466	2.02079	0.00000	0.22312	0.00065	0.09891	0.55516
25	0.19691	1.79274	0.00000	0.13002	0.00040	0.38132	0.50535
26	0.08075	1.83421	0.00000	0.13001	0.00027	0.20936	0.45004
27	0.01063	1.83555	0.00000	0.13003	0.00018	0.28945	0.39620
28	0.05226	1.72989	0.00000	0.13000	0.00011	0.01288	0.35880

Table S6 Best fitted parameters (χ_T, χ_S, τ and α) with the extended Debye model for complex **1** at 1500 Oe in the temperature range 8-23 K.

T/ K	χ_S / cm^3 mol^{-1}	χ_T / cm^3 mol^{-1}	τ/s	α
8	0.41724	6.19862	0.04136	0.27663
9	0.34977	5.40500	0.02251	0.24998
10	0.35960	4.79054	0.01314	0.21678
11	0.32325	4.37874	0.00843	0.21366
12	0.27833	4.03989	0.00568	0.21772
13	0.27000	3.73492	0.00388	0.21428
14	0.32126	3.44703	0.00278	0.19032
15	0.27657	3.26054	0.00200	0.20832
16	0.25331	3.05670	0.00140	0.21524
17	0.20000	2.89453	0.00098	0.23705
18	0.19978	2.73762	0.00069	0.24466
19	0.00136	2.61104	0.00041	0.29913
20	0.19993	2.47476	0.00032	0.27978
21	0.19971	2.36536	0.00021	0.29985
22	0.19912	2.25021	0.00013	0.29772
23	0.08490	2.15000	0.00008	0.29900

Table S7 Best fitted parameters (χ_T, χ_S, τ and α) with the extended Debye model for **1a** at 0 Oe in the temperature range 10-23 K.

T/ K	χ_S / cm^3 mol^{-1}	χ_T / cm^3 mol^{-1}	τ/s	α
10	0.09993	6.00001	0.01426	0.26351
11	0.09937	5.40199	0.00974	0.24141
12	0.09965	5.00008	0.00711	0.23657
13	0.10000	4.54777	0.00496	0.21809
14	0.05024	4.24061	0.00361	0.22556
15	0.06869	3.95476	0.00270	0.21805
16	0.15046	3.74274	0.00186	0.26408
17	0.02936	3.49873	0.00149	0.22971
18	0.09991	3.40018	0.00123	0.24572
19	0.07827	3.15082	0.00086	0.23618
20	0.09905	3.00003	0.00064	0.24526
21	0.10000	2.90019	0.00049	0.26837
22	0.07171	2.71374	0.00031	0.28031
23	0.09953	2.58948	0.00025	0.25674

Table S8 Best fitted parameters (χ_T, χ_S, τ and α) with the extended Debye model for **1a** at 1500 Oe in the temperature range 9-24 K.

T/ K	χ_S / cm^3 mol^{-1}	χ_T / cm^3 mol^{-1}	τ/s	α
9	0.04463	6.19995	0.07752	0.20774
10	0.00946	5.90020	0.05019	0.23803
11	0.00697	5.40891	0.03139	0.25047
12	0.05912	5.20034	0.02170	0.28110
13	0.02367	4.59964	0.01316	0.25588
14	0.01963	4.28759	0.00897	0.25744
15	0.02512	4.00213	0.00629	0.25106
16	0.03311	3.73565	0.00441	0.25127
17	0.03921	3.52582	0.00316	0.25778
18	0.00504	3.32428	0.00221	0.27499
19	0.09767	3.15008	0.00167	0.26514
20	0.10000	3.00000	0.00120	0.27618
21	0.09796	2.85286	0.00083	0.28817
22	0.09885	2.71940	0.00057	0.29684
23	0.11287	2.59190	0.00040	0.29320
24	0.09548	2.48243	0.00026	0.29976

Table S9 The shortest Dy-O bond lengths of some reported Dy^{III} tetranuclear complexes.

Complex	The shortest Dy-O bond (Å)
$[Dy_4(HL)_4(OAc)_2(H_2O)_2]\cdot(Et_3NH)_2$	2.241
$[(Cp^*_2Dy)_4(tz^{\cdot})_4]\cdot3(C_6H_6)$	No Dy-O bond
$[Dy_4(L)_2(OAc)_8(CH_3OH)_2]$	2.169
$[Dy_4(\mu_3\text{-}OH)_2L_6(acac)_4]\cdot2.5CH_3CN$	2.285
$[Dy_4(\mu_3\text{-}OH)_2L_6(tmhd)_4]\cdot2CH_3CN$	2.285
$[Dy_4(\mu_3\text{-}OH)_2L_6(beac)_4]\ CH_3CN$	2.232
$[Dy_4(vht)_4(MeOH)_8](NO_3)_4\cdot8.07MeOH\cdot0.65H_2O$	2.206

$[Dy_4(bzhdep\text{-}2H)_4(H_2O)_4(NO_3)_4]\cdot 6CH_3OH\cdot 6H_2O$	2.289
$[Dy_4(OH)_2(bpt)_4(NO_3)_4(OAc)_2]$	2.211
$[Dy_4Cl_2(\mu_3\text{-}OH)_2(\mu\text{-}OH)_2(2,2\text{-}bpt)_4(H_2O)_4]Cl_2\cdot 2H_2O\cdot 4EtOH$	2.252
$[Dy_4Br_2(\mu_3\text{-}OH)_2(\mu\text{-}OH)_2(2,2\text{-}bpt)_4(H_2O)_4]Cl_2\cdot 2H_2O\cdot 4EtOH$	2.243
$[Dy_4(HL)_2(L)_4(\mu_3\text{-}OH)_2]\ 5(MeOH)_2\cdot 7H_2O$	2.327
$[Dy_4(\mu_3\text{-}bpt)_4(\mu_3\text{-}OH)_2(\mu\text{-}OMe)_2(NO_3)_4]\cdot 3MeOH$	2.322
$[Dy_4(\mu_3\text{-}OH)_2(mdeaH)_2(piv)_8]$	2.370
$[Dy_4(\mu_3\text{-}OH)_2(bmh)_2(msh)_4Cl_2]$	2.298
$[Dy_4L_2(HL)_2(\mu_3\text{-}OH)_2(NO_3)_2](NO_3)_2\cdot 3CH_3CN\cdot 5H_2O$	2.308

Table S10 Energy barriers were obtained from the Arrhenius law fitting and Equation 1 of the out-of-phase (χ'') ac susceptibility data under zero dc field.

Relaxation processes	Orbach processes		Raman, QTM and Orbach processes				
	U_{eff}/k_B (K)	τ_0 (s)	q	C ($s^{-1}\cdot K^{-n}$)	n	U_{eff}/k_B (K)	τ_0 (s)
1	175(27)	1.7×10^{-8}	1.7	0.1	3.5	207(2)	5.1×10^{-9}
	319(11)	1.3×10^{-9}	0.3	2.3×10^{-4}	4.8	353(3)	4.6×10^{-10}
1a	151(14)	3.5×10^{-7}	1.5	9.3×10^{-3}	3.9	193(3)	1.1×10^{-7}

Table S11 Energy barriers were obtained from the Arrhenius law fitting and Equation 2 of the out-of-phase (χ'') ac susceptibility data under 1500 Oe dc field.

Relaxation processes	Orbach processes		Raman and Orbach processes			
	U_{eff}/k_B (K)	τ_0 (s)	C ($s^{-1}\cdot K^{-n}$)	n	U_{eff}/k_B (K)	τ_0 (s)
1	213(11)	7.9×10^{-9}	1.7×10^{-3}	4.6	245(1)	3.0×10^{-9}
1a	193(14)	1.0×10^{-7}	1.2×10^{-3}	4.3	230(1)	4.1×10^{-8}

Computational detail

For tetranuclear complex 1, we only need to calculate two types of individual Dy^{III} fragments (Dy1 and Dy2) due to the centrosymmetric structure (see Fig. S19). Complete-active-space self-consistent field (CASSCF) calculations on individual Dy^{III} fragments have been carried out with OpenMolcas[S1] program package. Each of individual Dy^{III} fragments in complex **1** was calculated keeping the experimentally determined structures of the corresponding compounds while replacing the other Dy^{III} ions with diamagnetic Lu^{III}.

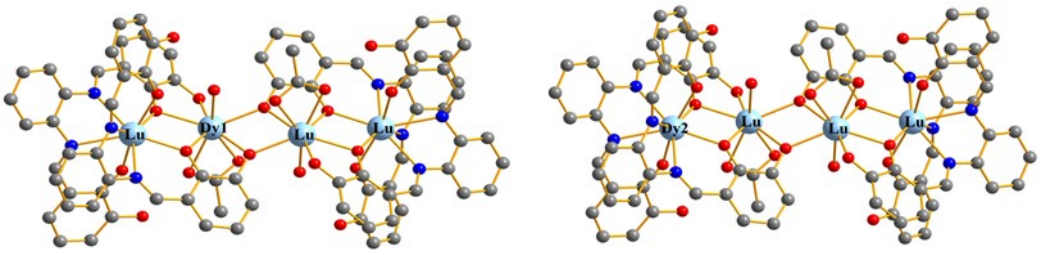

Fig. S19 Calculated model structures of individual Dy^{III} fragments of complex **1**; H atoms are omitted for clarify.

The basis sets for all atoms are atomic natural orbitals from the ANO-RCC library: ANO-RCC-VTZP for Dy^{III}; VTZ for close N and O; VDZ for distant atoms. The calculations employed the second order Douglas-Kroll-Hess Hamiltonian, where scalar relativistic contractions were taken into account in the basis set and the spin-orbit couplings were handled separately in the restricted active space state interaction (RASSI-SO) procedure.[S2, S3] For each individual Dy^{III} fragment, active electrons in 7 active orbitals include all *f* electrons (CAS(9 in 7 for Dy^{III})) in

the CASSCF calculation. To exclude all the doubts, we calculated all the roots in the active space. We have mixed the maximum number of spin-free state which was possible with our hardware (all from 21 sextets, 128 from 224 quadruplets, 130 from 490 doublets) for each fragment. SINGLE_ANISO[S4–S6] program was used to obtain the energy levels, *g* tensors, magnetic axes, *et al.* based on the above CASSCF/RASSI-SO calculations.

Table S12 Calculated energy levels (cm^{-1}), *g* (g_x, g_y, g_z) tensors and predominant m_J values of the lowest eight Kramers doublets (KDs) of individual Dy^{III} fragments for complex **1** using CASSCF/RASSI-SO with OpenMolcas.

KDs	Dy1			Dy2		
	E	*g*	m_J	*E*	*g*	m_J
1	0.0	0.002 0.004 19.645	±15/2	0.0	0.005 0.006 19.791	±15/2
2	197.1	0.016 0.036 16.630	±13/2	181.5	0.063 0.111 16.967	±13/2
3	351.4	1.071 2.629 10.831	±11/2	312.5	3.372 4.095 13.735	±1/2
4	384.7	10.375 5.976 1.448	±1/2	356.7	7.557 5.459 0.506	±11/2
5	430.6	11.057 6.116 1.102	±3/2	404.2	2.289 4.760 11.182	±3/2
6	480.7	1.531 2.604 14.690	±9/2	517.2	3.707 5.062 8.662	±5/2
7	544.9	0.088 0.304 17.822	±7/2	572.2	0.844 3.816 6.800	±7/2
8	609.5	0.111 0.284 19.143	±7/2	609.0	12.218 7.229 1.168	±9/2

Table S13 Wave functions with definite projection of the total moment | m_J > for the lowest eight KDs of individual Dy^{III} fragments for complex **1** using CASSCF/RASSI-SO with OpenMolcas.

	E/cm^{-1}	wave functions
Dy1	0.0	96.1%|±15/2>
	197.1	87.3%|±13/2>+8.6%|±9/2>
	351.4	49.6%|±11/2>+17.5%|±7/2>+14.4%|±3/2>+9.7%|±1/2>

	384.7	54%|±1/2>+12.9%|±3/2>+10.5%|±5/2>+7.8%|±11/2>+6.2%|±9/2>
	430.6	34.5%|±3/2>+33.2%|±5/2>+13.8%|±11/2>+13.6%|±9/2>
	480.7	28%|±9/2>+18.1%|±7/2>+16%|±1/2>+15.6%|±3/2>+10.5%|±5/2>+9.3% |±11/2>
	544.9	25.2%|±7/2>+20.9%|±5/2>+17.4%|±9/2>+16.9%|±1/2>+14.3%|±3/2>
	609.5	32.4%|±7/2>+25.4%|±9/2>+20.2%|±5/2>+9.9%|±11/2>+7.9%|±3/2>
Dy2	0.0	98.9%|±15/2>
	181.5	89.9%|±13/2>+6%|±11/2>
	312.5	52.2%|±1/2>+18.5%|±11/2>+14.3%|±3/2>+10.1%|±5/2>
	356.7	32.9%|±11/2>+21.8%|±3/2>+15.3%|±9/2>+15.3%|±1/2>+10.4%|±5/2>
	404.2	40.8%|±3/2>+21.7%|±1/2>+14%|±7/2>+11.8%|±9/2>+5.8%|±11/2>
	517.2	56.3%|±5/2>+23.8%|±11/2>+9.3%|±7/2>+3.7%|±13/2>
	572.2	39.8%|±7/2>+24.7%|±9/2>+15.5%|±3/2>+10.1%|±11/2>
	609.0	42.3%|±9/2>+31.8%|±7/2>+10.5%|±5/2>+8.7%|±1/2>

To fit the exchange interactions between Dy^{III} ions in complex **1**, we took two steps to obtain them. Firstly, we calculated individual Dy^{III} fragments using CASSCF/RASSI-SO to obtain the corresponding magnetic properties. Then, the exchange interaction between the magnetic centers was considered within the Lines model,[S7] while the account of the dipole-dipole magnetic coupling is treated exactly. The Lines model is effective and has been successfully used widely in the research field of *d* and *f*-elements single-molecule magnets.[S8, S9]

For complex **1**, we only consider the interactions between the nearest neighbour Dy^{III} ions. Thus, there only exist two types of $\tilde{J}$.

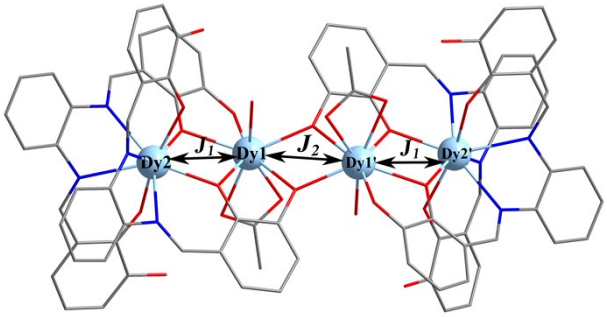

Fig. S20 Scheme of the Dy^{III}-Dy^{III} interactions in complex **1**.

The Ising exchange Hamiltonian for **1** is:

$$\hat{H}_{exch} = -\tilde{J}_1 \hat{S}_{Dy1} \hat{S}_{Dy2} - \tilde{J}_2 \hat{S}_{Dy1} \hat{S}_{Dy1'} \qquad \text{(S1)}$$

where $\tilde{J}_1 = 25\cos\varphi J_1$, φ is the angle between the anisotropy axes on sites Dy1 and Dy2, and J_1 is the Lines exchange coupling parameter. $\tilde{J}_2$ also has the similar expression. The $\hat{S}_{Dy}$ = 1/2 is the ground pseudospin on the Dy^{III} site. The total $\tilde{J}_{total}$ is the parameter of the total magnetic interaction ($\tilde{J}_{total} = \tilde{J}_{dipolar} + \tilde{J}_{exchange}$) between magnetic center ions. The dipolar magnetic couplings can be calculated exactly, while the Lines exchange coupling constants were fitted through comparison of the computed and measured magnetic susceptibilities using the POLY_ANISO program.[S4–S6]

Table S14. Fitted exchange coupling constant $\hat{J}_{exch}$ (cm^{-1}) through comparison of the computed and measured magnetic susceptibilities ($\chi_M T$-T) and magnetic hysteresis (M-H), respectively, the calculated dipole-dipole interaction $\hat{J}_{dip}$ and $\hat{J}_{total}$ (cm^{-1}) between magnetic center ions in **1**. The intermolecular interaction zJ' of **1** was fitted to 0.01 and −0.01 cm^{-1} for $\chi_M T$-T and M-H, respectively.

		$\hat{J}_{exch}$	$\hat{J}_{dip}$	$\hat{J}_{total}$
$\chi_M T$-T	J_1	−2.3	−0.6	−2.9
	J_2	−4.5	0.8	−3.7
M-H	J_1	−1.4	−0.6	−2.0
	J_2	−5.0	0.8	−4.2

We gave the exchange energies (cm^{-1}), the energy differences between each exchange doublet Δ_t (cm^{-1}) and the main values of the g_z for the lowest eight exchange doublets of **1** in Table S15. The g_z value of the ground exchange state of **1** is 0.000, which confirms that the Dy^{III}-Dy^{III} interactions in **1** are all antiferromagnetic.

Table S15. Exchange energies E (cm^{-1}), the energy difference between each exchange doublets Δ_t (cm^{-1}) and the main values of the g_z for the lowest eight exchange doublets of complex **1**.

M-H			
exchange doublets	*E*	Δ_t	g_z
1	0.000000000000	1.300×10^{-11}	0.000
	0.000000000013		
2	2.142895749844	3.530×10^{-10}	39.577
	2.142895750197		
3	2.218523208370	4.200×10^{-11}	0.004
	2.218523208412		
4	3.137172429161	3.250×10^{-10}	39.581
	3.137172429486		
5	4.442156938476	5.550×10^{-10}	39.289
	4.442156939026		
6	5.436512804906	4.950×10^{-10}	39.289
	5.436512805401		
7	6.342320455299	8.620×10^{-10}	50.565
	6.342320456161		
8	6.597909054517	1.840×10^{-10}	60.530
	6.597909054701		

For complex 2, there are two types of J.

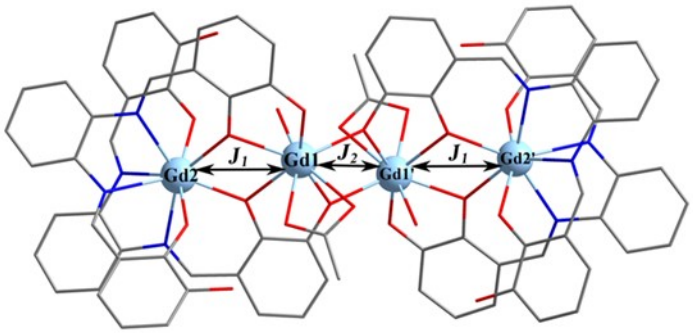

Fig. S21 Scheme of the Gd^{III}-Gd^{III} interactions in complex **2.**

The Isotropic exchange Hamiltonian is:

$$\hat{H}_{exch} = -J_1(S_{Gd1}S_{Gd2} + S_{Gd1'}S_{Gd2'}) - J_2S_{Gd1}S_{Gd1'} \quad (1)$$

J_1 and J_2 are the parameters of the total magnetic coupling constants between the magnetic centers. S_{Gd} = 7/2 is the ground spin on the Gd^{III} ions. The Lines exchange coupling constants J_1 and J_2 were fitted through comparison of the computed and measured magnetic susceptibilities using the POLY_ANISO program.

Table S16. Fitted the total magnetic coupling parameters J_1 and J_2 (cm^{-1}) through comparison of the computed and measured magnetic susceptibilities ($\chi_M T$-T) and magnetic hysteresis (M-H) respectively between magnetic center ions in **2**. The intermolecular interaction zJ' of **2** was fitted to −0.01 and −0.02 cm^{-1} for $\chi_M T$-T and M-H, respectively.

	J_1	J_2
$\chi_M T$-T	–0.15	–0.14
M-H	–0.22	–0.22

References:

S1 Galván, I. F.; Vacher, M.; Alavi, A.; Angeli, C.; Aquilante, F.; Autschbach, J.; Bao, J. J.; Bokarev, S. I.; Bogdanov, N. A.; Carlson, R. K.; Chibotaru, L. F.; Creutzberg, J.; Dattani, N.; Delcey, M. G.; Dong, S. S.; Dreuw, A.; Freitag, L.; Frutos, L. M.; Gagliardi, L.; Gendron, F.; Giussani, A.; González, L.; Grell, G.; Guo, M. Y.; Hoyer, C. E.; Johansson, M.; Keller, S.; Knecht, S.; Kovacevic, G.; Källman, E.; Manni, G. L.; Lundberg, M.; Ma, Y. J.; Mai, S.; Malhado, J. P.; Malmqvist, P. Å.; Marquetand, P.; Mewes, S. A.; Norell, J.; Olivucci, M.; Oppel, M.; Phung, Q. M.; Pierloot, K.; Plasser, F.; Reiher, M.; Sand, A. M.; Schapiro, I.; Sharma, P.; Stein, C. J.; Sørensen, L. K.; Truhlar, D. G.; Ugandi, M.; Ungur, L.; Valentini, A.; Vancoillie, S.; Veryazov, V.; Weser, O.; Wesołowski, T. A.; Widmark, Per-Olof.; Wouters, S.; Zech, A.; Zobel, J. P.; Lindh. R. *J. Chem. Theory Comput.* **2019**, *15*, 5925–5964.

S2 Malmqvist, P. Å.; Roos, B. O.; Schimmelpfennig, B. *Chem. Phys. Lett.,* **2002**, *357,* 230–240.

S3 Heß, B. A.; Marian, C. M.; Wahlgren, U.; Gropen, O. *Chem. Phys. Lett.,* **1996**, *251,* 365–371.

S4 Chibotaru, L. F.; Ungur, L.; Soncini, A. *Angew. Chem., Int. Ed*. **2008**, *47*, 4126–4129.

S5 Ungur, L.; Van den Heuvel, W.; Chibotaru, L. F. *New J. Chem.* **2009**, *33*, 1224–1230.

S6 Chibotaru, L. F.; Ungur, L.; Aronica, C.; Elmoll, H.; Pilet, G.; Luneau, D. *J. Am. Chem. Soc*. **2008**, *130*, 12445–12455.

S7 Lines, M. E. *J. Chem. Phys*. **1971**, *55*, 2977−2984.

S8 Mondal, K. C.; Sundt, A.; Lan, Y. H.; Kostakis, G. E.; Waldmann, O.; Ungur, L.; Chibotaru, L. F.; Anson, C. E.; Powell, A. K. *Angew. Chem., Int. Ed.* **2012**, *51*, 7550−7554.

S9 Langley, S. K.; Wielechowski, D. P.; Vieru, V.; Chilton, N. F.; Moubaraki, B.; Abrahams, B. F.; Chibotaru, L. F.; Murray, K. S. *Angew. Chem., Int. Ed.* **2013**, *52*, 12014–12019.